Applied Catalysis B: Environmental 224 (2018) 360–367

Contents lists available at ScienceDirect

Applied Catalysis B: Environmental

journal homepage: www.elsevier.com/locate/apcatb

Research Paper

Sub-2 nm Pt-decorated $Zn_{0.5}Cd_{0.5}S$ nanocrystals with twin-induced homojunctions for efficient visible-light-driven photocatalytic H_2 evolution

Boon-Junn Ng[a], Lutfi Kurnianditia Putri[a], Xin Ying Kong[a], Katrina Pui Yee Shak[b], Pooria Pasbakhsh[c], Siang-Piao Chai[a,*], Abdul Rahman Mohamed[d]

[a] Multidisciplinary Platform of Advanced Engineering, Chemical Engineering Discipline, School of Engineering, Monash University, Jalan Lagoon Selatan, 47500 Bandar Sunway, Selangor, Malaysia
[b] Department of Chemical Engineering, Lee Kong Chian Faculty of Engineering and Science, Universiti Tunku Abdul Rahman, Jalan Sungai Long, Bandar Sungai Long, Cheras, 43000 Kajang, Selangor, Malaysia
[c] Mechanical Engineering Discipline, School of Engineering, Monash University, Jalan Lagoon Selatan, 47500 Bandar Sunway, Selangor, Malaysia
[d] Low Carbon Economy (LCE) Group, School of Chemical Engineering, Universiti Sains Malaysia, Engineering Campus, Seri Ampangan, 14300 Nibong Tebal, Pulau Pinang, Malaysia

ARTICLE INFO

Keywords:
Twinned $Zn_{0.5}Cd_{0.5}S$
Sub-2 nm Pt
Water splitting
Photocatalyst
Hydrogen

ABSTRACT

Pseudobinary $Zn_xCd_{1-x}S$ semiconductor with zinc blende/wurtzite (ZB/WZ) twin-induced crystal structure has been regarded as one of the best pristine sulfide photocatalysts for H_2 evolution *via* water splitting. While the synthesis of this nano-twin photocatalyst is at the forefront of research, the incorporation of co-catalyst to improve photocatalytic activities through synergistic properties has rarely been reported. Loading well-dispersed ultrasmall platinum (Pt) with controlled sizes is the pivotal element in maximizing atom-utilization efficiencies by downsizing the noble metal clusters. In this contribution, we report the fabrication of highly dispersed sub-2 nm Pt decorated twinned $Zn_{0.5}Cd_{0.5}S$ nanocrystals and their excellent photocatalytic H_2 evolution in both acidic and alkaline sacrificial reagents. The high visible-light-driven H_2 evolution rates of the most active sample (denoted as 8Pt-$Zn_{0.5}Cd_{0.5}S$) in 0.1 M Na_2S/0.1 M Na_2SO_3 (pH = 12.94) and 0.15 M ascorbic acid (pH = 2.24) are measured to be 114.3 μmol h^{-1} (AQY:7.15%) and 164.9 μmol h^{-1} (AQY:8.56%), respectively, which render ca. 4.9- and 27.9-fold enhancement over pristine twinned $Zn_{0.5}Cd_{0.5}S$. The presence of homojunctions (within ZB and WZ segments) and heterojunctions (between Pt and twinned $Zn_{0.5}Cd_{0.5}S$) impart an efficient spatial charge separation and provide more active sites for highly efficient photocatalytic H_2 production.

1. Introduction

Owing to the onslaught of energy crisis and environmental problems on a worldwide scale, a transition in the energy sector to utilize clean and renewable carrier is imperative to mitigate those concerns [1,2]. Hydrogen (H_2) is worth noting as the potential front runner of future energy mix ascribed to its non-polluting nature and high energy density [3,4]. Photocatalytic water splitting has been a hot research topic due to its intriguing and sustainable approach to harvest H_2 fuel using solar energy [5–7]. Hitherto, there has been an incessant endeavor devoted to develop highly efficient H_2-evolving photocatalyst, in particular metal chalcogenides, attributed to their ideal band gap and thermodynamically favorable relative band positions for H_2 evolution [8]. However, further commercial development of the photocatalysts remains as a daunting challenge as pristine metal sulfides generally suffer from rapid charge recombination and severe photocorrosion [9].

As of late, ternary metal chalcogenides, for instance $Zn_xCd_{1-x}S$, have emerged as a viable candidate to surmount the aforementioned limitations owing to its tunable band gap, stability to photocorrosion and remarkable photocatalytic properties [10]. Even so, $Zn_xCd_{1-x}S$ with single crystal phase is still plagued by poor spatial charge isolation which decreases the lifetime of photogenerated carriers [11]. Twinning in nanocrystals by forming homojunctions between two different crystal phases within a single semiconductor can promote effective electron-hole pairs separation and suppress recombination [12]. A recreation of these nano-twin structures can be witnessed in $Zn_{0.5}Cd_{0.5}S$ with alternative arrangement of zinc blende/wurtzite (ZB/WZ) segments that are periodically arranged in twinning superlattice alignment [13]. The "back-to-back" potentials imparted by the ingenious arrangement of parallel ZB/WZ segments in twinned $Zn_{0.5}Cd_{0.5}S$ nanocrystals can substantially improve the electron transport nature and confer efficient spatial isolation of photogenerated charge carriers

* Corresponding author.
E-mail address: chai.siang.piao@monash.edu (S.-P. Chai).

http://dx.doi.org/10.1016/j.apcatb.2017.10.005
Received 17 July 2017; Received in revised form 9 September 2017; Accepted 3 October 2017
Available online 06 October 2017

[14,15]. Nevertheless, there is still large research space to further propel the electron-hole pairs separation and incorporate more active sites on the surface.

Employing co-catalysts onto semiconductors has been demonstrated to be an effective way to introduce catalytic active sites and serve as electron traps to suppress charge recombination [16]. Noble metal such as platinum (Pt) is generally regarded as the best H_2-evolving co-catalyst which can diminish the kinetic barrier for interfacial electron transfer and facilitate photocatalytic H_2 activities [17]. However, the deposition of well-dispersed Pt nanoparticles with controlled sizes to maximize the atom-utilization efficiencies has often been overlooked [18,19]. Downsizing the Pt clusters to ultrasmall nanoparticles endows a compelling strategy to incorporate co-catalyst with minimum aggregation [20]. This paves way to maximize the utilization of Pt to compensate for its high cost and limited reserves.

Herein, we report a facile synthetic route to fabricate fine-tuned twinned $Zn_{0.5}Cd_{0.5}S$ nanocrystals assembled with highly dispersed sub-2 nm Pt nanoparticles, which can achieve a remarkably high photocatalytic H_2 production under visible light. This result shows a stark improvement as compared to the sample with photo-deposited Pt, which implies the influence of Pt dispersion on photocatalytic performance. It is worth mentioning that the sub-2 nm Pt decorated twinned $Zn_{0.5}Cd_{0.5}S$ sample is one of the few photocatalysts reported that can exhibit high photocatalytic H_2 evolution under both acidic and alkaline conditions.

2. Experimental

2.1. Materials

Zinc acetate dihydrate, $Zn(Ac)_2{\cdot}2H_2O$ (98%, Friendemann Schmidt Chemical), cadmium acetate dihydrate, $Cd(Ac)_2{\cdot}2H_2O$ (98%, Sigma Aldrich), thioacetamide (98%, Sigma Aldrich), sodium hydroxide, NaOH (98%, Sigma Aldrich), hexachloroplatinic (IV) acid hexahydrate, $H_2PtCl_6{\cdot}6H_2O$ (99.9%, Acros Organics) and ethanol (Grade AR 96%, Friendemann Schmidt Chemical) were used as received without further purification.

2.2. Preparation of twinned $Zn_{0.5}Cd_{0.5}S$ nanocrystals

$Zn_{0.5}Cd_{0.5}S$ nanocrystals with twinned induced homojunctions were synthesized *via* a co-precipitation-hydrothermal strategy. Typically, 10 mmol of $Zn(Ac)_2{\cdot}2H_2O$ and 10 mmol of $Cd(Ac)_2{\cdot}2H_2O$ were added into 20 mL of DI water and stirred for 15 min. 25 mmol of thioacetamide pre-dissolved in 20 mL of DI water was then added dropwise into the mixture and stirred for another 15 min. Later on, the mixture was added with 10 mL of 4 M NaOH and further stirred for 30 min. Subsequently, the solution was transferred into a Teflon-lined stainless steel autoclave and subjected to hydrothermal process at 180 °C for 24 h. After the solution was cooled down to room temperature, the precipitates were collected using centrifugation and the as-obtained solid was then washed with ethanol and DI water 3 times each.

2.3. Preparation of sub-2 nm Pt-decorated $Zn_{0.5}Cd_{0.5}S$ nanocrystals

Deposition of sub-2 nm Pt on twinned $Zn_{0.5}Cd_{0.5}S$ nanocrystals was carried out using a simple liquid phase mixing with post N_2 annealing. Firstly, 0.25 g of the as-synthesized twinned $Zn_{0.5}Cd_{0.5}S$ powder was dispersed in 75 mL of DI water by stirring and sonication for 15 min each. The solution was then heated up to 70 °C. Successively, 10 mg of $H_2PtCl_6{\cdot}6H_2O$ pre-dissolved in 5 mL of DI water was added dropwise into the solution and further stirred for 4–10 h. Afterwards, the precipitates were collected using centrifugation and rinsed with ethanol and DI water 3 times each. The as-obtained solid was then dried in vacuum oven at 60 °C. Next, the dried sample was post calcined at 130 °C for 1 h under N_2 environment. The resulting products were denoted as xPt-$Zn_{0.5}Cd_{0.5}S$ (x = 4, 6, 8 and 10 h, respectively).

2.4. Preparation of Pt-$Zn_{0.5}Cd_{0.5}S$ nanocrystals using photo-deposition

In brief, 0.25 g of the as-prepared twinned $Zn_{0.5}Cd_{0.5}S$ powder was dispersed in 150 mL of 20 vol% aqueous methanol solution by stirring and sonication for 15 min each. 2 mg of $H_2PtCl_6{\cdot}6H_2O$ pre-dissolved in 5 mL of DI water was then added into the solution and deaerated with N_2 gas for 30 min. Later on, the solution was irradiated with visible light using a 500 W Xe arc lamp (CHF-XM-500 W) equipped with an optical filter ($\lambda > 400$ nm) for 6 h. Subsequently, the precipitates were collected using centrifugation and washed with ethanol and DI water 3 times each. The dried sample was then post calcined at 130 °C for 1 h under N_2 flow. The resulting product was denoted as Pt-$Zn_{0.5}Cd_{0.5}S$-PD.

2.5. Materials characterization

The surface morphology and elemental composition were examined by transmission electron microscopy (TEM) and energy-dispersive X-ray (EDX) spectroscopy. High resolution TEM (HRTEM) images were taken using a JEOL JEM-2100F microscope operated at 200 kV. The elemental contents of the as-prepared samples were also obtained *via* inductively coupled plasma-mass spectrometry (ICP-MS) using Agilent 7900 ICP-MS. The crystallographic properties of the samples were investigated using X-ray diffraction (XRD) analysis on a Bruker D8 Discover X-ray diffractometer with Ni-filtered Cu Kα radiation ($\lambda = 1.54056$ Å) at a scan rate of $0.02^{\circ}\,s^{-1}$. X-ray photoelectron spectroscopy (XPS) measurements were performed using a scanning X-ray microprobe PHI Quantera II (Ulvac-PHI, INC.) with monochromatic Al-Kα ($h\nu = 1486.6$ eV) X-ray source. Prior to deconvolution, all binding energies were referenced to adventitious carbon signal (C 1s peak) at 284.6 eV. Meanwhile, UV–vis diffused reflectance spectrums of the samples were evaluated using a Cary 100 UV–vis spectrophotometer (Agilent) equipped with an integrated sphere and $BaSO_4$ was employed as a reflectance standard. Lastly, the photoluminescence (PL) emission spectra were obtained using a fluorescence spectrometer (Perkin Elmer, LS55).

2.6. Electrochemical analysis

The electrochemical measurements (transient photocurrent and Nyquist plots) were carried out by a CHI 6005E electrochemical workstation with a conventional three-electrode quartz cell. The working electrode was prepared by drop-casting the as-prepared samples in ethanol suspension (5 mg/mL) on a fluorine-doped tin oxide (FTO) substrate with an active area of 1 cm^2, while Pt serves as the counter electrode and Ag/AgCl saturated with 3 M KCl as the reference electrode. During the measurements, 0.5 M Na_2SO_4 solution was employed as the electrolyte and the working electrode was irradiated with a lamp-to-sample distance of 15 cm using a 500 W Xe arc lamp (CHF-XM-500 W) equipped with an optical filter ($\lambda > 400$ nm).

2.7. Evaluation of photocatalytic activities

The photcatalytic H_2 evolution was conducted in a Pyrex side-irradiated vessel with a continuous N_2 flow at atmospheric pressure. Each photocatalyst sample (0.03 g) was dispersed in 120 mL sacrificial reagent aqueous solution containing 0.1 M Na_2S and 0.1 M Na_2SO_3 (pH = 12.94) or 0.15 M ascorbic acid (pH = 2.24) under vigorous stirring. Prior to the photocatalytic activity, the reaction system was evacuated by purging N_2 gas at a high flow rate for 30 min. A 500 W Xe arc lamp (CHF-XM-500 W) equipped with an optical filter ($\lambda > 400$ nm) was used as a visible light source. The gas sampling port of the system is directly connected to a gas chromatography (Agilent 7890A, TCD, Ar carrier gas) for online measurement of the product gas at an hourly auto sampling interval. For stability testing, the sample

Table 1
Analytical data of energy-dispersive X-ray (EDX) spectroscopy of twinned $Zn_{0.5}Cd_{0.5}S$.

Sample	Weight Percentage (wt%)			Atomic Percentage (at%)		
	Zn	Cd	S	Zn	Cd	S
Twinned $Zn_{0.5}Cd_{0.5}S$	26.96	46.69	23.45	23.24	23.41	41.22

Table 2
Analytical data of inductively coupled plasma-mass spectroscopy (ICP-MS) of the as-prepared Pt-decorated twinned $Zn_{0.5}Cd_{0.5}S$.

Entry	Sample	Pt Weight Percentage (wt%)
1	4Pt-$Zn_{0.5}Cd_{0.5}S$	0.29
2	6Pt-$Zn_{0.5}Cd_{0.5}S$	0.38
3	8Pt-$Zn_{0.5}Cd_{0.5}S$	0.48
4	10Pt-$Zn_{0.5}Cd_{0.5}S$	0.61
5	Pt-$Zn_{0.5}Cd_{0.5}S$-PD	0.52

was recovered and washed with DI water after each run before recycling and dispersing into fresh sacrificial solution for the next run. The apparent quantum yield (AQY) was calculated by measuring the photocatalytic H_2 evolution under monochromatic light using 420 nm band pass filter (light spectrum is given in Fig. S1 of the Supporting information), according to the following equation:

$$AQY = \frac{2 \times \text{Number of evolved } H_2 \text{ molecules}}{\text{Number of incident photons}} \times 100\%$$

3. Results and discussion

Twinned $Zn_{0.5}Cd_{0.5}S$ nanocrystals decorated with various loadings of Pt nanoparticles were synthesized *via* a two-step liquid phase mixing with different reaction time and post N_2 annealing using the same amount of Pt precursor. The resulting samples were denoted as xPt-$Zn_{0.5}Cd_{0.5}S$ (x corresponds to mixing time of 4, 6, 8 and 10 h, respectively). For comparison, $Zn_{0.5}Cd_{0.5}S$ with photo-deposited Pt (denoted as Pt-$Zn_{0.5}Cd_{0.5}S$-PD) was prepared as a control sample. Detailed procedures of materials preparation are mentioned in the Experimental Section. The elemental composition of pristine twinned $Zn_{0.5}Cd_{0.5}S$ was determined by EDX, which revealed a Zn:Cd:S molar ratio that was very close to the expected stoichiometry of 1:1:2 (Table 1). Besides, the varying Pt contents from 0.29 wt% to 0.61 wt% of the Pt-decorated $Zn_{0.5}Cd_{0.5}S$ samples were obtained from ICP-MS, as depicted in the tabulated data from Table 2.

To provide an insight on the morphology of the best sample, 8Pt-$Zn_{0.5}Cd_{0.5}S$ was firstly characterized using TEM. Fig. 1A delineates the presence of regular strip-like structures on the surface of nanoparticles. As disclosed by the HRTEM image in Fig. 1B, the strips were identified as nano-twin structures with alternative arrangement of ZB/WZ segments. In addition, the coherent twin boundaries in parallel alignment can be clearly visualized, indicating the formation of twin-induced homojunctions, which was further supported by SAED pattern shown in the inset of Fig. 1B. A closer observation of the HRTEM image reveals the uniform dispersion of ultrasmall Pt nanoparticles with a mean size of 1.6 nm on $Zn_{0.5}Cd_{0.5}S$ with minimum aggregation (Fig. 1C). The lattice spacing measurement of 0.33 nm can be assigned to the (111) diffraction plane of $Zn_{0.5}Cd_{0.5}S$ nanocrystals [12,15]. The inset of Fig. 1C shows that the ultrasmall Pt nanoparticle is a single crystal and displays an intimate interfacial contact with $Zn_{0.5}Cd_{0.5}S$, implying the formation of interactive heterojunction. The Pt loading of 8Pt-$Zn_{0.5}Cd_{0.5}S$ was determined to be 0.48 wt% (Table 2). Besides, HRTEM images of 4Pt-$Zn_{0.5}Cd_{0.5}S$, 6Pt-$Zn_{0.5}Cd_{0.5}S$ and 10Pt-$Zn_{0.5}Cd_{0.5}S$ showed the average particle sizes of Pt were 1.4, 1.5 and 1.9 nm, respectively (Fig. S2). A plausible charge transfer mechanism was postulated in Fig. 1D, strongly elucidate the synergistic effect of both homojunctions and heterojunctions in driving efficient charge isolation to improve the

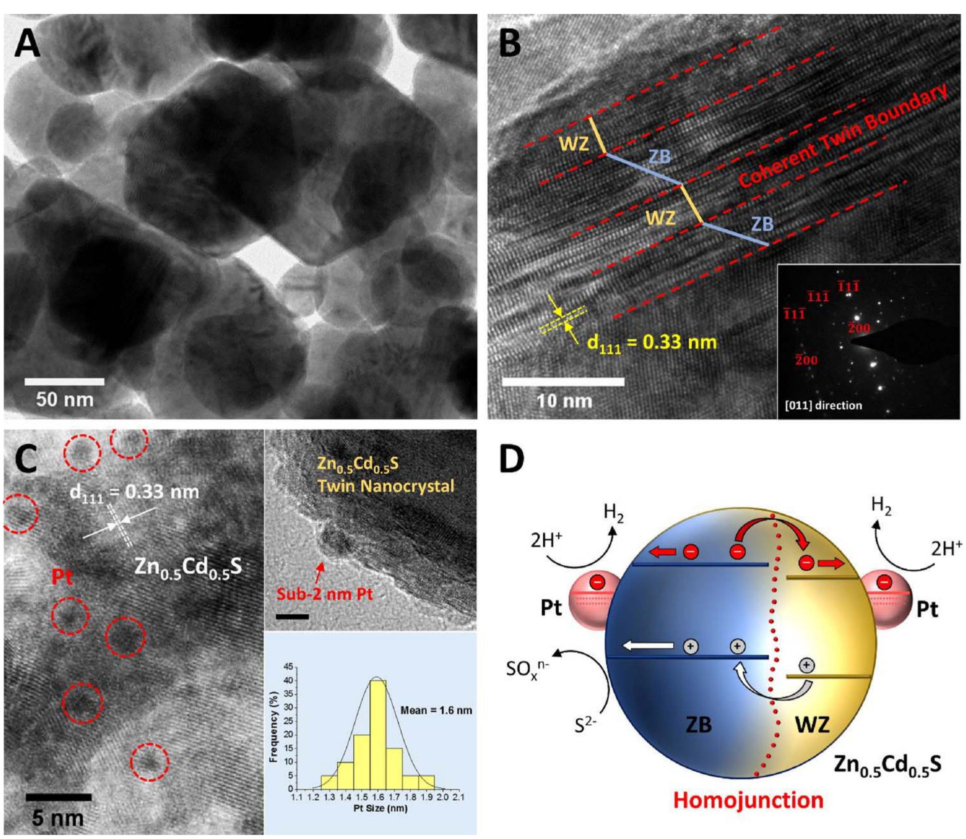

Fig. 1. (A) Representative TEM image of 8Pt-$Zn_{0.5}Cd_{0.5}S$ nanocrystals. HRTEM images of 8Pt-$Zn_{0.5}Cd_{0.5}S$ showing (B) coherent twin boundaries of alternative ZB/WZ segments and SAED (inset), and (C) ultrasmall Pt nanoparticles decorated on twinned $Zn_{0.5}Cd_{0.5}S$; insets show the enlarged image of single-crystalline Pt (scale bar: 2 nm) and Pt particle size distribution plot. (D) Proposed electron/hole transfer mechanism for Pt-decorated twinned $Zn_{0.5}Cd_{0.5}S$ system.

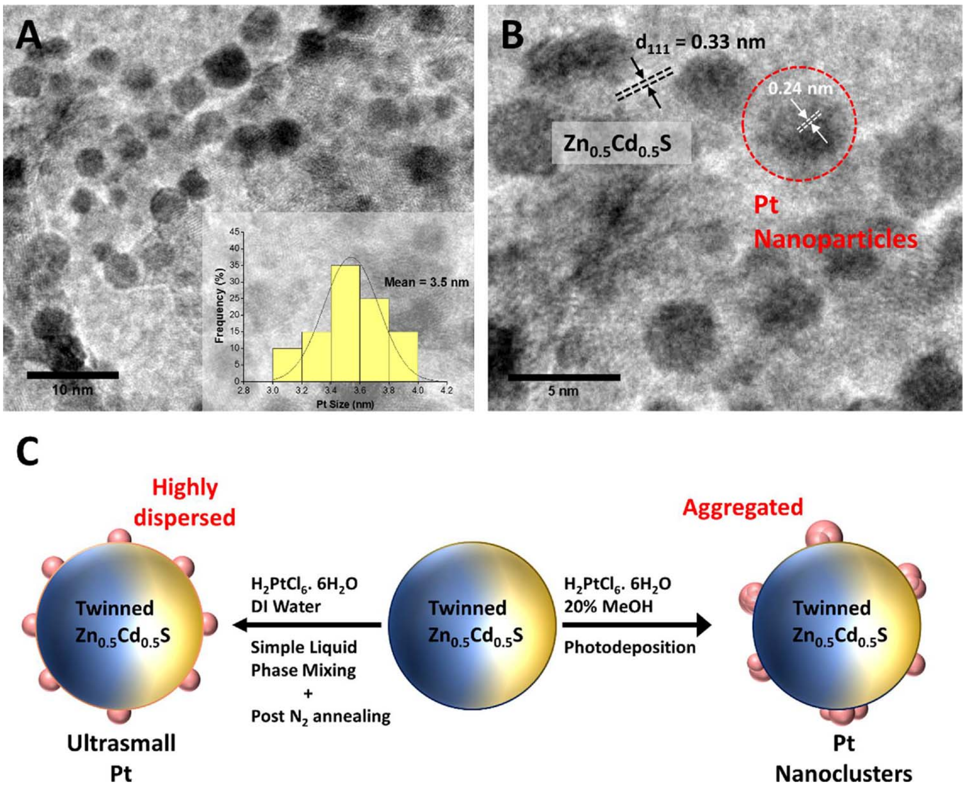

Fig. 2. (A) Representative HRTEM image of Pt-$Zn_{0.5}Cd_{0.5}S$-PD nanocrystals and Pt particle size distribution plot (inset). (B) Enlarged HRTEM image showing heterojunctions and lattice spacings. (C) Schematic illustration of synthesis process for twinned $Zn_{0.5}Cd_{0.5}S$ nanocrystals decorated with highly dispersed ultrasmall Pt nanoparticles and aggregated Pt nanoclusters.

photocatalytic activities.

To attest the significance of the synthesis method on the dispersion of Pt, control sample was then examined under TEM. Fig. 2A depicts a fairly aggregated upsized Pt nanoclusters with a mean size of 3.5 nm from Pt-$Zn_{0.5}Cd_{0.5}S$-PD sample. The overlapping of two lattice fringes indicates the formation of heterojunctions between $Zn_{0.5}Cd_{0.5}S$ and Pt with lattice spacings of 0.33 and 0.24 nm, respectively (Fig. 2B) [13,21]. The Pt content of Pt-$Zn_{0.5}Cd_{0.5}S$-PD was measured to be 0.52 wt%, as disclosed in Table 2. The results reveal that the size and dispersion of Pt are inextricably linked to the two different synthetic routes, as shown in Fig. 2C. Most of the Pt nanoparticles in the sample using photo-deposition method were subjected to aggregation and hence formed nanoclusters. The remnant metals which are not directly attached on $Zn_{0.5}Cd_{0.5}S$ will not be available for photocatalytic reaction, resulting in lesser utilization of Pt nanoparticles. Conversely, the method of liquid phase mixing with post N_2 sintering at low temperature endow a more precise and controlled condition to incorporate Pt nanoparticles. In this case, the deposited Pt nanoparticles are smaller in size and have more germane interfacial contact with $Zn_{0.5}Cd_{0.5}S$ nanocrystals.

XRD patterns of the twinned $Zn_{0.5}Cd_{0.5}S$, xPt-$Zn_{0.5}Cd_{0.5}S$ and Pt-$Zn_{0.5}Cd_{0.5}S$-PD nanocrystals are shown in Fig. 3. The diffraction peaks of the samples can be well-indexed to display multiphase crystal properties that are comprised of cubic phase of zinc-blende ZnS and hexagonal phase of wurtzite CdS [11,15]. All the samples delineate apparent peaks shift towards higher angle, indicating the incorporation of Zn^{2+} into the lattice of CdS. The decrease in lattice fringes is ascribed to the smaller radius of Zn^{2+} ion as compared to Cd^{2+} [9]. This result ascertains the successful formation of twinned $Zn_{0.5}Cd_{0.5}S$ nanocrystals with two different crystal phases. However, the lack of Pt diffraction peak is attributed to low metal loadings.

The chemical states of twinned $Zn_{0.5}Cd_{0.5}S$ and 8Pt-$Zn_{0.5}Cd_{0.5}S$ samples were investigated through XPS in order to study the interfacial interaction between deposited Pt and $Zn_{0.5}Cd_{0.5}S$ nanocrystals. Fig. 4A presents full XPS spectra of both samples, indicating the presence of Zn, Cd, S and Pt as the major elements. High resolution XPS spectra of Zn

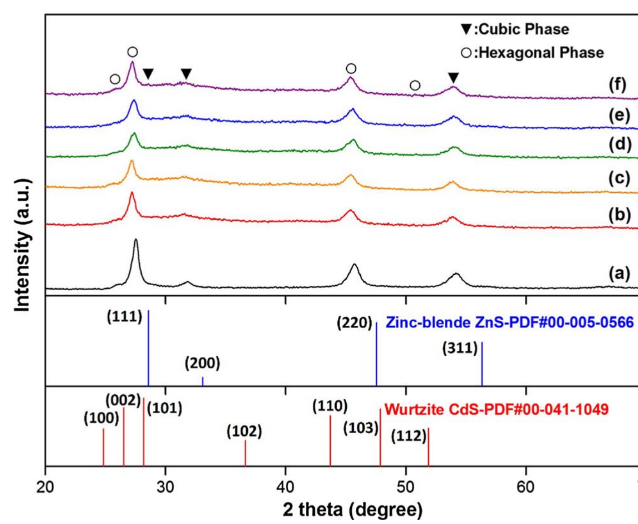

Fig. 3. XRD patterns of (a) twinned $Zn_{0.5}Cd_{0.5}S$, (b) 4Pt-$Zn_{0.5}Cd_{0.5}S$, (c) 6Pt-$Zn_{0.5}Cd_{0.5}S$, (d) 8Pt-$Zn_{0.5}Cd_{0.5}S$, (e) 10Pt-$Zn_{0.5}Cd_{0.5}S$ and (f) Pt-$Zn_{0.5}Cd_{0.5}S$-PD nanocrystals.

2p reveals the presence of Zn $2p_{3/2}$ and Zn $2p_{1/2}$ at 1021.9 eV and 1044.7 eV, respectively (Fig. 4B). Fig. 4C shows the high resolution XPS spectra of Cd 3d where the peaks at 404.9 eV and 411.8 eV could be assigned to Cd $3d_{5/2}$ and Cd $3d_{3/2}$, which is analogous to Cd^{2+} in CdS [22]. Besides, the high resolution of S 2p XPS spectrums of both samples are exhibited in Fig. 4D and E, in which the peaks are observed at binding energies of 161.6 and 161.4 eV, respectively. A slight shift in binding energies of Zn 2p, Cd 3d and S 2p of 8Pt-$Zn_{0.5}Cd_{0.5}S$ sample to a higher value as compared to twinned $Zn_{0.5}Cd_{0.5}S$ was attributed to the presence of interfacial interaction between S and Pt [15]. Furthermore, the deconvoluted XPS spectra of Pt 4f demonstrates the presence of Pt $4f_{5/2}$ (72.0 and 73.1 eV) and Pt $4f_{7/2}$ (75.2 and 76.1 eV) in 8Pt-$Zn_{0.5}Cd_{0.5}S$ (Fig. 4F).

The optical properties of the samples were investigated using

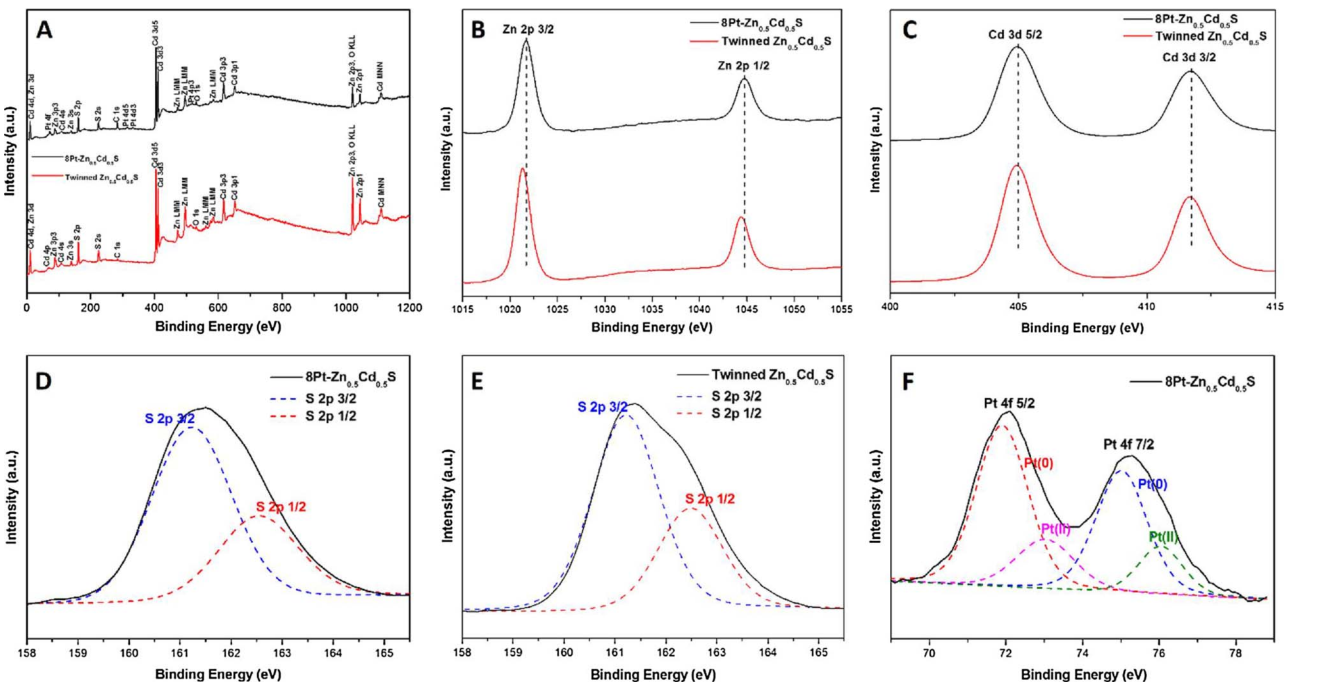

Fig. 4. (A) Full XPS spectra of twinned $Zn_{0.5}Cd_{0.5}S$ and 8Pt-$Zn_{0.5}Cd_{0.5}S$. (B) Zn 2p, and (C) Cd 3d XPS spectra of $Zn_{0.5}Cd_{0.5}S$ and 8Pt-$Zn_{0.5}Cd_{0.5}S$. (D) S 2p XPS spectra of 8Pt-$Zn_{0.5}Cd_{0.5}S$. (E) S 2p XPS spectra of twinned $Zn_{0.5}Cd_{0.5}S$. (F) Pt 4f XPS spectra of 8Pt-$Zn_{0.5}Cd_{0.5}S$.

UV–vis DRS, as depicted in Fig. 5. Pristine twinned $Zn_{0.5}Cd_{0.5}S$ nanocrystals displayed a sharp absorption edge at 520 nm with a corresponding band gap of 2.38 eV (Fig. 5A and B). The incorporation of Pt nanoparticles showed a slight red-shift in the absorption edge, which exhibited absorption onset of ca. 550 nm for all the Pt-decorated samples (Fig. 5A). According to the KM function presented in Fig. 5B, the band gaps of the Pt-deposited samples were estimated to be 2.25 eV. The trend shown in the UV–vis spectra suggest that the enhanced background absorption in the visible region is attributed to the increase in Pt loading. This observation was further supported by the occurrence of gradual color change in the samples from yellow to grayish yellow with increasing Pt loadings (inset of Fig. 5A).

The photocatalytic H_2 performance of the samples were tested under both alkaline (0.1 M Na_2S/0.1 M Na_2SO_3, pH = 12.94) and acidic (0.15 M ascorbic acid, pH = 2.24) sacrificial conditions. As delineated in Fig. 6, 8Pt-$Zn_{0.5}Cd_{0.5}S$ demonstrated significantly higher gas production, with remarkable H_2 evolution rates of 114.3 and 164.9 μmol h^{-1} in alkaline and acidic sacrificial solutions, respectively. This leads to exceptional 4.9- (alkaline) and 27.9-fold (acid) enhancement in H_2 production as compared to pristine twinned $Zn_{0.5}Cd_{0.5}S$, signifying ultrasmall Pt nanoparticles as crucial co-catalysts to suppress the charge recombination and provide catalytic active sites. Besides, the augmentation in H_2 yield of 8Pt-$Zn_{0.5}Cd_{0.5}S$ sample in contrast to the sluggish H_2 activity of Pt-$Zn_{0.5}Cd_{0.5}S$-PD eminently highlights the importance of downsized Pt nanoparticles in maximizing the atom-utilization efficiencies to improve the photocatalytic performance. The H_2 activities of the Pt-decorated samples prepared by liquid phase mixing and post annealing method were in the order of 8Pt-$Zn_{0.5}Cd_{0.5}S$ > 6Pt-$Zn_{0.5}Cd_{0.5}S$ > 10Pt-$Zn_{0.5}Cd_{0.5}S$ > 4Pt-$Zn_{0.5}Cd_{0.5}S$, in which 8Pt-$Zn_{0.5}Cd_{0.5}S$ was identified as the sample with the most optimized Pt loading. Therefore, it can be deduced that low content of Pt did not implement sufficient active sites while an excessive loading of Pt can cause shielding effect which decrease the light absorption of twinned $Zn_{0.5}Cd_{0.5}S$. Consequently, the apparent quantum yield (AQY) of 8Pt-$Zn_{0.5}Cd_{0.5}S$ in alkaline and acidic sacrificial reagents were measured to be 7.15 and 8.56%, respectively. The time courses of H_2 evolution of

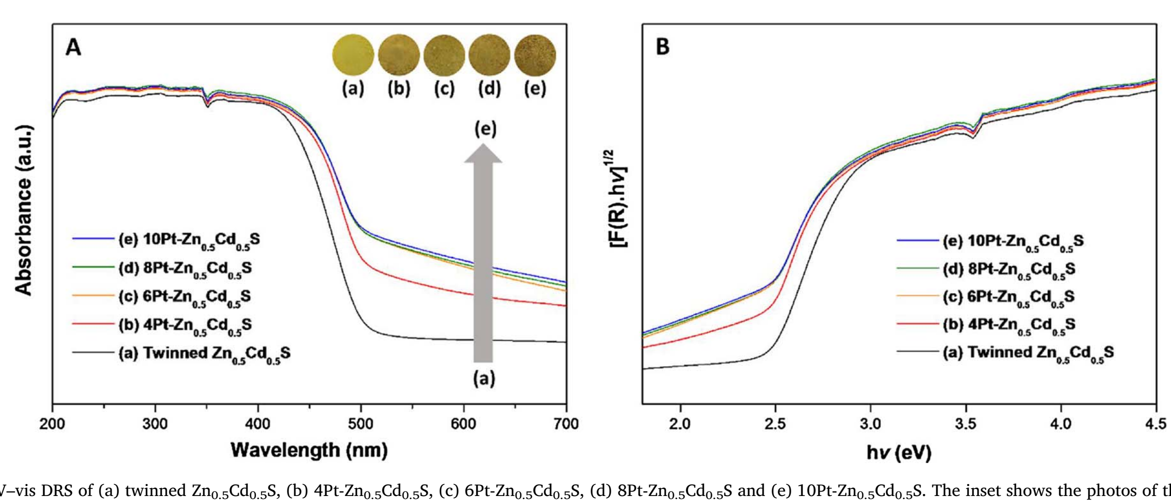

Fig. 5. (A) UV–vis DRS of (a) twinned $Zn_{0.5}Cd_{0.5}S$, (b) 4Pt-$Zn_{0.5}Cd_{0.5}S$, (c) 6Pt-$Zn_{0.5}Cd_{0.5}S$, (d) 8Pt-$Zn_{0.5}Cd_{0.5}S$ and (e) 10Pt-$Zn_{0.5}Cd_{0.5}S$. The inset shows the photos of the samples. (B) Plot of transformed KM function vs hν for the corresponding samples.

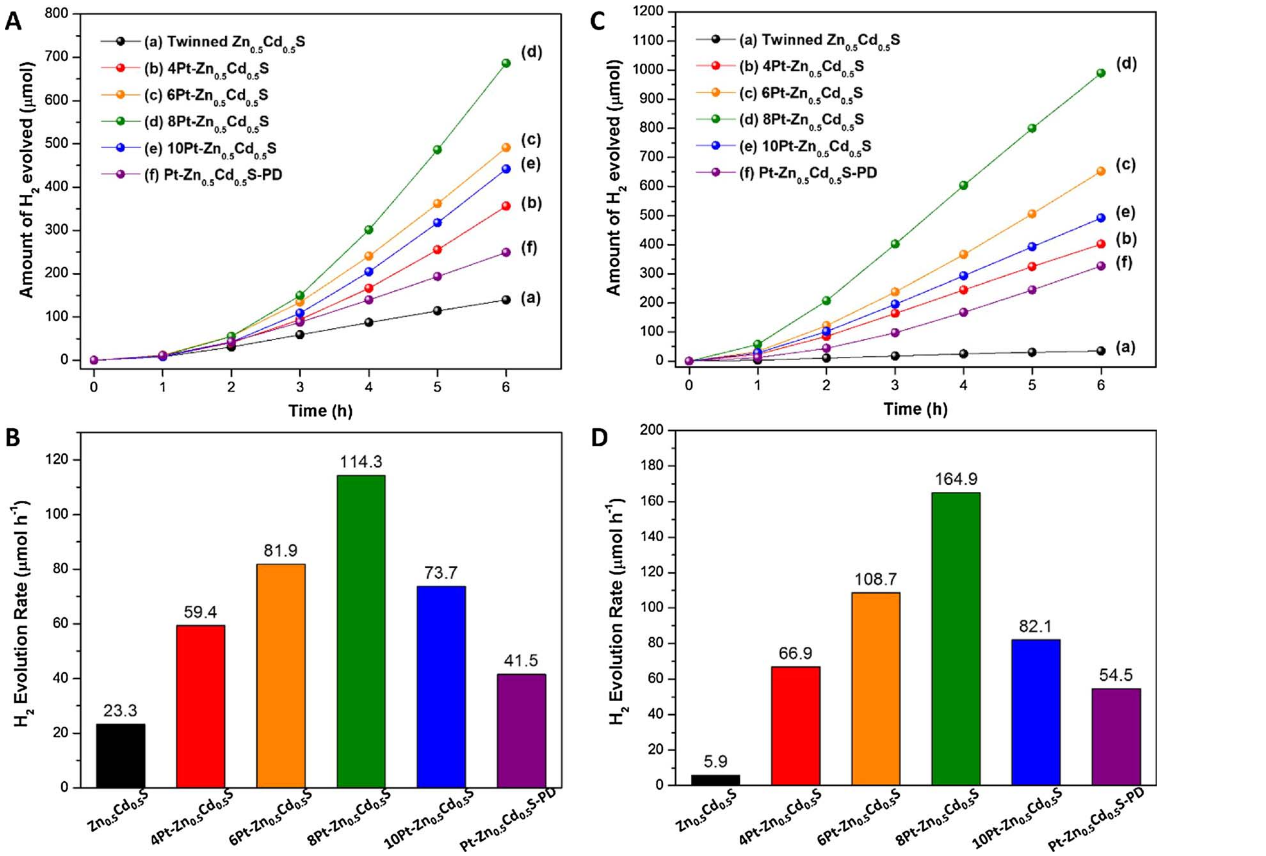

Fig. 6. (A) Time courses of H_2 evolution, and (B) corresponding H_2 yield in 0.1 M Na_2S/0.1 M Na_2SO_3 (pH = 12.94). (C) Time courses of H_2 evolution, and (D) corresponding H_2 yield in 0.15 M ascorbic acid (pH = 2.24).

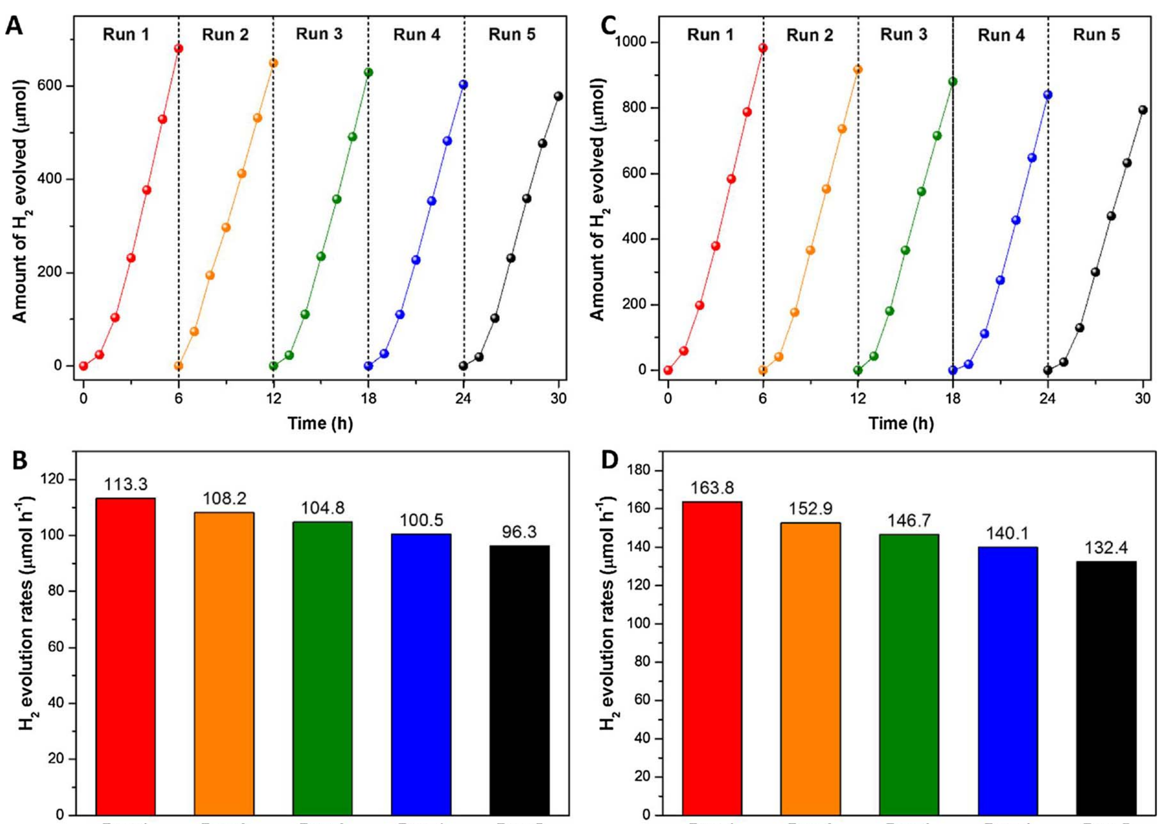

Fig. 7. Photostability tests of 8Pt-$Zn_{0.5}Cd_{0.5}S$ for recycling runs of H_2 evolution under visible light: (A) Time courses of cyclic H_2 evolution, and (B) corresponding H_2 yield in 0.1 M Na_2S/0.1 M Na_2SO_3. (C) Time courses of cyclic H_2 evolution, and (D) corresponding H_2 yield in 0.15 M ascorbic acid.

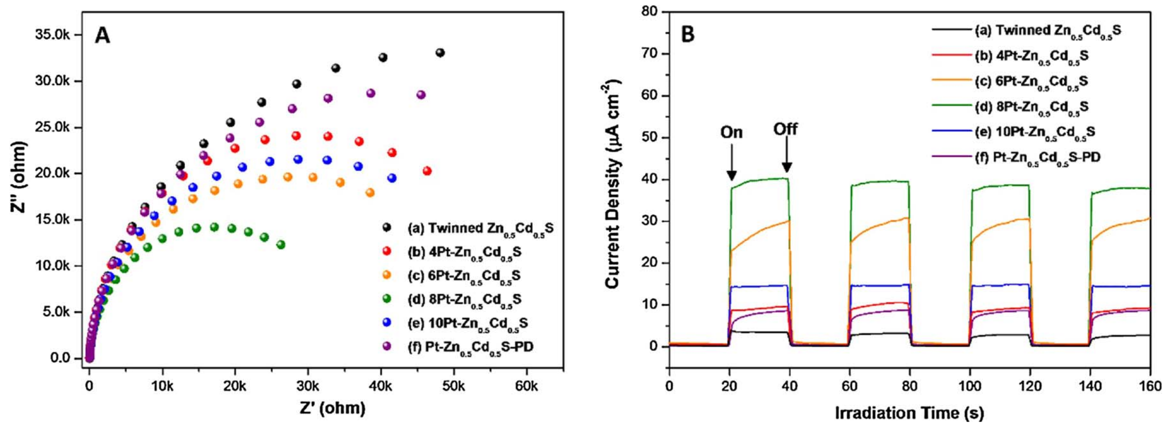

Fig. 8. (A) Nyquist impedance plots, and (B) transient photocurrent responses of (a) twinned $Zn_{0.5}Cd_{0.5}S$, (b) 4Pt-$Zn_{0.5}Cd_{0.5}S$, (c) 6Pt-$Zn_{0.5}Cd_{0.5}S$, (d) 8Pt-$Zn_{0.5}Cd_{0.5}S$, (e) 10Pt-$Zn_{0.5}Cd_{0.5}S$ and (f) Pt-$Zn_{0.5}Cd_{0.5}S$-PD.

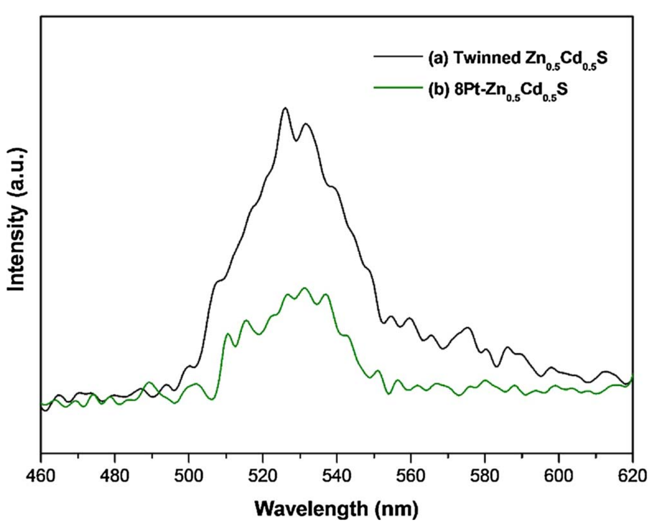

Fig. 9. PL spectra of (a) twinned $Zn_{0.5}Cd_{0.5}S$ and (b) 8Pt-$Zn_{0.5}Cd_{0.5}S$.

8Pt-$Zn_{0.5}Cd_{0.5}S$ under the irradiation of monochromatic light at 420 nm is depicted in Fig. S3. A comparison of real-time H_2 evolution between 8Pt-$Zn_{0.5}Cd_{0.5}S$ and Pt-$Zn_{0.5}Cd_{0.5}S$-PD in 0.1 M Na_2S/0.1 M Na_2SO_3 and the excellent H_2 activity of 8Pt-$Zn_{0.5}Cd_{0.5}S$ in 0.15 M ascorbic acid are shown in Movie S1 and S2 of the Supporting Information.

8Pt-$Zn_{0.5}Cd_{0.5}S$ was examined by TEM and XRD analyses after photocatalytic reaction. As shown in Fig. S4, the morphology and crystallinity of 8Pt-$Zn_{0.5}Cd_{0.5}S$ were preserved after reaction in both sacrificial solutions. In addition, it is noteworthy that 8Pt-$Zn_{0.5}Cd_{0.5}S$ maintained reactivity of 85.0 and 80.8% in alkaline and acidic conditions after five repeated photocatalytic reactions for a total of 30 h under similar experimental conditions (Fig. 7). This shows that the sample possesses high photostability and recyclability. Furthermore, control experiments of photocatalytic H_2 production on ZnS, CdS and twinned $Zn_{0.5}Cd_{0.5}S$ were conducted to ascertain the effect of homojunctions on $Zn_{0.5}Cd_{0.5}S$ nano-twin structures in driving higher gas evolution (Fig. S5). XRD patterns of ZnS, CdS and twinned $Zn_{0.5}Cd_{0.5}S$ were depicted in Fig. S6. The "back-to-back" potentials formed at the twinning superlattice of ZB/WZ with type-II staggered band alignment improves the charge isolation as compared to ZnS and CdS alone. Further separation of electron-hole pairs can be driven by the heterojunctions between Pt and twinned $Zn_{0.5}Cd_{0.5}S$, in which Pt can facilitate the movement of electrons that are initially constrained in the bulky catalyst and promote higher H_2 evolution.

EIS Nyquist plots were employed to further elucidate the charge transfer behaviors of the samples. As disclosed in Fig. 8A, the smaller arc radius of 8Pt-$Zn_{0.5}Cd_{0.5}S$ sample indicates a lower interfacial layer resistance with accelerated electron transfer [23]. Fig. 8B shows the transient photocurrent measurements of the samples at a bias voltage of 0.1 V under visible light irradiation. As expected, 8Pt-$Zn_{0.5}Cd_{0.5}S$ displays a stark enhancement of photocurrent density as compared to the others, indicating the incorporation of highly dispersed ultrasmall Pt can promote effective charge separation and prolong time lifetime of photogenerated carriers. Besides, the weakening of PL intensity of 8Pt-$Zn_{0.5}Cd_{0.5}S$ as compared to twinned $Zn_{0.5}Cd_{0.5}S$ strongly entrench its high efficiency of photogenerated carriers isolation and the suppression of electron-hole pairs recombination (Fig. 9).

4. Conclusions

In summary, we have successfully devised sub-2 nm Pt-decorated twinned $Zn_{0.5}Cd_{0.5}S$ nanocrystals with high efficiencies for water splitting in alkaline and acidic conditions. The highly dispersed Pt nanoparticles with a mean size of 1.6 nm maximize the atom-utilization efficiencies, resulted in a massive 4.9- and 27.9-fold augmentation of the photocatalytic H_2 evolution over twinned $Zn_{0.5}Cd_{0.5}S$ in both sacrificial environments. The synergistic effects of both homojunctions and heterojunctions enhanced spatial charge isolation and dramatically improved the photocatalytic activities. To date, highly active metal chalcogenides for water splitting under both acidic and alkaline solutions are sparsely documented. As a whole, our findings highlight the significance of downsized Pt nanoparticles combined with twinned $Zn_{0.5}Cd_{0.5}S$ nanocrystals as an intriguing photcatalyst for better insights to develop highly-efficient devices in photocatalytic H_2 production.

Acknowledgements

This work was funded by the Ministry of Higher Education (MOHE) Malaysia under Fundamental Research Grant Scheme (FRGS) (Ref. no.: FRGS/1/2016/TK02/MUSM/02/1) and Universiti Sains Malaysia (USM) under NanoMITe Long-term Research Grant Scheme (LRGS) (Ref. no.: 203/PJKIMIA/6720009).

Appendix A. Supplementary data

Supplementary data associated with this article can be found, in the online version, at http://dx.doi.org/10.1016/j.apcatb.2017.10.005.

References

[1] W.-J. Ong, L.-L. Tan, Y.H. Ng, S.-T. Yong, S.-P. Chai, Graphitic carbon nitride (g-C_3N_4)-based photocatalysts for artificial photosynthesis and environmental remediation: are we a step closer to achieving sustainability? Chem. Rev. 116 (2016) 7159–7329.

[2] X.Y. Kong, Y.Y. Choo, S.-P. Chai, A.K. Soh, A.R. Mohamed, Oxygen vacancy induced Bi_2WO_6 for the realization of photocatalytic CO_2 reduction over the full solar spectrum: from the UV to the NIR region, Chem. Commun. 52 (2016) 14242–14245.

[3] Q. Wang, T. Hisatomi, Y. Suzuki, Z. Pan, J. Seo, M. Katayama, T. Minegishi, H. Nishiyama, T. Takata, K. Seki, A. Kudo, T. Yamada, K. Domen, Particulate photocatalyst sheets based on carbon conductor layer for efficient Z-scheme pure-water splitting at ambient pressure, J. Am. Chem. Soc. 139 (2017) 1675–1683.

[4] L. Yao, D. Wei, Y. Ni, D. Yan, C. Hu, Surface localization of CdZnS quantum dots onto 2D g-C_3N_4 ultrathin microribbons: highly efficient visible light-induced H_2-generation, Nano Energy 26 (2016) 248–256.

[5] J. Chen, X.J. Wu, L. Yin, B. Li, X. Hong, Z. Fan, B. Chen, C. Xue, H. Zhang, One-pot synthesis of CdS nanocrystals hybridized with single-layer transition-metal dichalcogenide nanosheets for efficient photocatalytic hydrogen evolution, Angew. Chem. 54 (2015) 1210–1214.

[6] L.K. Putri, B.-J. Ng, W.-J. Ong, H.W. Lee, W.S. Chang, S.-P. Chai, Heteroatom nitrogen- and boron-doping as a facile strategy to improve photocatalytic activity of standalone reduced graphene oxide in hydrogen evolution, ACS Appl. Mater. Interface 9 (2017) 4558–4569.

[7] M. Zheng, Y. Ding, L. Yu, X. Du, Y. Zhao, In situ grown pristine cobalt sulfide as bifunctional photocatalyst for hydrogen and oxygen evolution, Adv. Funct. Mater. 27 (2017) 1605846.

[8] K. Iwashina, A. Iwase, Y.H. Ng, R. Amal, A. Kudo, Z-Schematic water splitting into H_2 and O_2 using metal sulfide as a hydrogen-evolving photocatalyst and reduced graphene oxide as a solid-state electron mediator, J. Am. Chem. Soc. 137 (2015) 604–607.

[9] W.-J. Ong, J.-J. Yeong, L.-L. Tan, B.T. Goh, S.-T. Yong, S.-P. Chai, Synergistic effect of graphene as a co-catalyst for enhanced daylight-induced photocatalytic activity of $Zn_{0.5}Cd_{0.5}S$ synthesized *via* an improved one-pot co-precipitation-hydrothermal strategy, RSC Adv. 4 (2014) 59676–59685.

[10] K. Li, R. Chen, S.L. Li, S.L. Xie, L.Z. Dong, Z.H. Kang, J.C. Bao, Y.Q. Lan, Engineering $Zn_{1-x}Cd_xS$/CdS heterostructures with enhanced photocatalytic activity, ACS Appl. Mater. Interface 8 (2016) 14535–14541.

[11] H. Du, K. Liang, C.Z. Yuan, H.L. Guo, X. Zhou, Y.F. Jiang, A.W. Xu, Bare $Cd_{1-x}Zn_xS$ ZB/WZ heterophase nanojunctions for visible light photocatalytic hydrogen production with high efficiency, ACS Appl. Mater. Interface 8 (2016) 24550–24558.

[12] Y.Y. Hsu, N.T. Suen, C.C. Chang, S.F. Hung, C.L. Chen, T.S. Chan, C.L. Dong, C.C. Chan, S.Y. Chen, H.M. Chen, Heterojunction of zinc blende/wurtzite in $Zn_{1-x}Cd_xS$ solid solution for efficient solar hydrogen generation: X-ray absorption/diffraction approaches, ACS Appl. Mater. Interface 7 (2015) 22558–22569.

[13] M. Liu, D. Jing, Z. Zhou, L. Guo, Twin-induced one-dimensional homojunctions yield high quantum efficiency for solar hydrogen generation, Nat. Commun. 4 (2013) 2278.

[14] M. Liu, L. Wang, G. Lu, X. Yao, L. Guo, Twins in $Cd_{1-x}Zn_xS$ solid solution: highly efficient photocatalyst for hydrogen generation from water, Energy Environ. Sci. 4 (2011) 1372.

[15] J. Song, H. Zhao, R. Sun, X. Li, D. Sun, An efficient hydrogen evolution catalyst composed of palladium phosphorous sulphide ($PdP_{\sim 0.33}S_{\sim 1.67}$) and twin nanocrystal $Zn_{0.5}Cd_{0.5}S$ solid solution with both homo- and hetero-junctions, Energy Environ. Sci. 10 (2017) 225–235.

[16] L.-L. Tan, W.-J. Ong, S.-P. Chai, A.R. Mohamed, Noble metal modified reduced graphene oxide/TiO_2 ternary nanostructures for efficient visible-light-driven photoreduction of carbon dioxide into methane, Appl. Catal. B 166–167 (2015) 251–259.

[17] M. Luo, P. Lu, W. Yao, C. Huang, Q. Xu, Q. Wu, Y. Kuwahara, H. Yamashita, Shape and composition effects on photocatalytic hydrogen production for Pt-Pd alloy cocatalysts, ACS Appl. Mater. Interface 8 (2016) 20667–20674.

[18] Q. Chen, Y. Yang, Z. Cao, Q. Kuang, G. Du, Y. Jiang, Z. Xie, L. Zheng, Excavated cubic platinum-tin alloy nanocrystals constructed from ultrathin nanosheets with enhanced electrocatalytic activity, Angew. Chem. 55 (2016) 9021–9025.

[19] C. Wang, H. Daimon, T. Onodera, T. Koda, S. Sun, A general approach to the size- and shape-controlled synthesis of platinum nanoparticles and their catalytic reduction of oxygen, Angew. Chem. 47 (2008) 3588–3591.

[20] X. Li, W. Bi, L. Zhang, S. Tao, W. Chu, Q. Zhang, Y. Luo, C. Wu, Y. Xie, Single-atom Pt as co-catalyst for enhanced photocatalytic H_2 evolution, Adv. Mater. 28 (2016) 2427–2431.

[21] I. Vamvasakis, B. Liu, G.S. Armatas, Size effects of platinum nanoparticles in the photocatalytic hydrogen production over 3D mesoporous networks of CdS and Pt nanojunctions, Adv. Funct. Mater. 26 (2016) 8062–8071.

[22] B.-J. Ng, L.K. Putri, L.-L. Tan, P. Pasbakhsh, S.-P. Chai, All-solid-state Z-scheme photocatalyst with carbon nanotubes as an electron mediator for hydrogen evolution under simulated solar light, Chem. Eng. J. 316 (2017) 41–49.

[23] X.Y. Kong, W.L. Tan, B.-J. Ng, S.-P. Chai, A.R. Mohamed, Harnessing Vis–NIR broad spectrum for photocatalytic CO_2 reduction over carbon quantum dots-decorated ultrathin Bi_2WO_6 nanosheets, Nano Res. 10 (2017) 1720–1731.